

## Article

# Synergetic Mechanism of Multiple Industrial Solid Waste-Based Geopolymer Binder for Soil Stabilization: Optimization Using D-Optimal Mixture Design

Xiaoli Wang <sup>1,2</sup>, Xiancong Wang <sup>1</sup>, Pingfeng Fu <sup>1,\*</sup> , Bolan Lei <sup>1</sup>, Jinjin Shi <sup>3,4</sup> and Miao Xu <sup>3,4</sup>

<sup>1</sup> School of Civil and Resources Engineering, University of Science and Technology Beijing, Beijing 100083, China; xiaoliwang@ustb.edu.cn (X.W.); runner17@163.com (X.W.); leibolan1999@163.com (B.L.)

<sup>2</sup> State Key Laboratory of Mineral Processing, Beijing 100160, China

<sup>3</sup> Cangzhou Municipal Engineering Company Limited, Cangzhou 061000, China; czszjsk@126.com (J.S.); czszxm1989@163.com (M.X.)

<sup>4</sup> Road Materials and Technology Engineering Research Center of Hebei Province, Cangzhou 061000, China

\* Correspondence: pffu@ces.ustb.edu.cn

**Abstract:** In order to improve the comprehensive utilization rate of industrial solid waste and the road quality, a novel low-carbon and environmental friendly soil stabilizer is proposed. In this study, steel slag (SS), carbide slag (CS), blast furnace slag (BFS), fly ash (FA), and desulfurized gypsum (DG) were used as raw materials to develop a multiple industrial solid waste-based soil stabilizer (MSWSS). The optimal mix ratio of the raw materials determined by D-optimal design was as follows: 5% SS, 50% CS, 15% BFS, 15% DG, and 15% FA. The 7-day unconfined compressive strength (UCS) of MSWSS-stabilized soil was 1.7 MPa, which was 36% higher than stabilization with ordinary portland cement (OPC) and met the construction requirements of highways. After 7 days of curing, the UCS of MSWSS-stabilized soil was significantly higher than that in the OPC group. X-ray powder diffraction (XRD), thermogravimetric analysis (TGA), and scanning electron microscopy (SEM) analysis indicated that the prominent hydration products were ettringite (AFt) and C-S-H gel. The results showed that an amount of AFt and C-S-H were formed in the initial stage of curing, resulting in a rapid improvement in early UCS. As the curing proceeded, the content of AFt and C-S-H increased constantly and grew intertwined with each other, which lead to the denser microstructure of stabilized soil and better mechanical strength.

**Keywords:** soil stabilization; industrial solid waste; D-optimal mixture approach; hydration mechanism



**Citation:** Wang, X.; Wang, X.; Fu, P.; Lei, B.; Shi, J.; Xu, M. Synergetic Mechanism of Multiple Industrial Solid Waste-Based Geopolymer Binder for Soil Stabilization: Optimization Using D-Optimal Mixture Design. *Processes* **2024**, *12*, 436. <https://doi.org/10.3390/pr12030436>

Academic Editor: Jacopo Donnini

Received: 26 January 2024

Revised: 10 February 2024

Accepted: 15 February 2024

Published: 21 February 2024



**Copyright:** © 2024 by the authors. Licensee MDPI, Basel, Switzerland. This article is an open access article distributed under the terms and conditions of the Creative Commons Attribution (CC BY) license (<https://creativecommons.org/licenses/by/4.0/>).

## 1. Introduction

Rapid urbanization has led to an exponential increase in the amount of solid waste that is generated. According to the report of the World Bank Group, global cities generate 2.01 billion tons of solid waste each year, including industrial waste, agricultural waste, and domestic waste. It is expected to increase to 3.40 billion tons per year by 2050 [1]. According to the statistics, only about 13.5% of solid waste is recycled globally [1]. Landfills and incineration are the two main solid waste disposal methods. However, these conventional treatments waste land resources, release harmful gases, and cause a negative impact on the economy, environment, and human health [2–4].

On the other hand, the development of urban transportation has brought challenges to the road construction industry [5,6]. The quality of pavement depends on the mechanical properties of the underlying soil, including strength, compressibility, permeability, etc. [7–9]. One of the effective ways to improve road quality is to use soil stabilizers. Traditional soil stabilizers are cement, lime, and coal fly ash, which are characterized by lower costs and being less time consuming [8,10,11]. However, although the soil solidified using cement exhibits high

early strength, its later strength development is limited. In contrast, soil solidified with lime and coal fly ash shows lower early compressive strength [12,13]. Additionally, the production process of these materials generates a large amount of carbon dioxide, accelerating global warming. The carbon dioxide emissions from cement production account for approximately 8% of global carbon dioxide emissions [14–17]. Therefore, environmentally friendly, efficient, and sustainable soil stabilizers should be explored as alternatives for pavement construction.

Recently, non-traditional stabilizers, especially cementitious materials based on multiple industrial solid wastes, have received more attention due to their low carbon emissions, low cost, low energy consumption, and better sustainability [18–22].

Steel slag (SS) and blast furnace slag (BFS) are the industrial solid waste generated in the process of steelmaking, and their major components are CaO, SiO<sub>2</sub>, and Al<sub>2</sub>O<sub>3</sub> [23–25]. In 2021, the SS output in China exceeded 120 million tons, but its comprehensive utilization was only about 20% [26]. Carbide slag (CS) is the predominant by-product resulting from the hydrolysis of calcium carbide during acetylene production, which is mainly composed of CaOH [23]. It is predicted that the annual production of CS exceeds 50 million tons in China, with a utilization rate is less than 30% [27]. Desulfurized gypsum (DG) is an industrial waste generated from smelters, large-scale enterprise boilers, and the desulfurization of flue gas in thermal power plants [28]. The output of DG in 2019 was approximately 130 million tons [29]. The main component of DG is CaSO<sub>4</sub>·2H<sub>2</sub>O, which also contains impurities such as CaCO<sub>3</sub> and CaSO<sub>3</sub>. Fly ash (FA) is a major solid waste emitted from thermal power plants [30,31]. The global annual production is estimated at 360 million tons [32], while China's annual output is about 800–900 million tons [33]. FA contains many toxic elements including Pb, As, Se, and Cr, and is considered to be a hazardous waste to the environment and human health [34,35].

From a chemical composition point of view, these industrial solid wastes (including SS, BFS, CS, DG, and FA) exhibit higher pozzolanic activity and alkalinity and can be used as raw materials for the preparation of geopolymers [21,36]. This is especially the case with CS, which, as an alkaline industrial solid waste, has the same main components and can be considered as a substitute for lime [37]. A geopolymer can interact with soil particles to form a cementitious gel through a pozzolanic reaction. The addition of CS, as an alkaline resource, provides OH<sup>−</sup> and Ca<sup>2+</sup>. Under alkaline conditions, the dissolution of aluminum and silica mineral components can be activated and react with Ca(OH)<sub>2</sub> to generate C-S-H, which can reduce pores and increase the compressive strength and stiffness of soil [38]. Several studies have been conducted on the utilization of industrial solid waste as soil stabilizers [19,29,39–43]. However, few studies investigated the action mechanisms of multiple industrial solid wastes as soil solidifiers, e.g., five different industrial solid wastes. The advantages of various solid wastes can be complemented to improve the utilization rate effectively and reduce costs.

In the present study, a novel low-carbon and environmentally friendly soil stabilizer is proposed in order to improve the comprehensive utilization efficiency of industrial solid waste and reduce environmental pollution. Steel slag (SS), carbide slag (CS), blast furnace slag (BFS), fly ash (FA), and desulfurized gypsum (DG) were used as raw materials to formulate a multiple industrial solid waste-based soil stabilizer (MSWSS). The D-optimal mixture design approach was utilized to determine the optimal formulation of the various raw materials for the MSWSS, which can reduce the number of experiments and costs [44]. The mechanical characteristics of the stabilized soil were evaluated using the unconfined compressive strength (UCS) test and compared with conventional soil stabilizers. The micromorphology of solidified soil and hydration mechanisms were investigated by using X-ray diffraction (XRD), scanning electron microscopy (SEM), and thermogravimetric analysis (TGA).

## 2. Materials and Methods

### 2.1. Materials

The test soil used in this study was collected from Cangzhou, Hebei Province, China, and had such characteristics as a small plasticity index, poor stability when exposed to

water, low strength, and the inability to be directly used as base for the construction of pavement. The characteristics of the test soil are provided in Table 1.

**Table 1.** Physical and mechanical properties of the test soil.

| Natural Water Content /% | Optimum Water Content/% | Maximum Dry Density/g·cm <sup>-3</sup> | Plastic Limit /% | Liquid Limit /% | Plasticity Index |
|--------------------------|-------------------------|--|------------------|-----------------|------------------|
| 7.22                     | 14.40                   | 1.85                                   | 25.10            | 40.28           | 15.18            |

The raw materials used to produce the MSWSS included CS, BFS, SS, FA, and DG, which were collected from the following companies: Hebei Jinniu Chemical Co., Ltd., Xingtai, China; Cangzhou Zhongtie Equipment Manufacturing Material Co., Ltd., Cangzhou, China; and Shenhua Group Guohua Power Plant, Yongzhou, China. The chemical compositions of the test soil and the raw materials are listed in Table 2, while the XRD patterns of the raw materials are shown in Figure 1. It can be seen from the results that SiO<sub>2</sub> (52.93%) comprised the largest proportion of the test soil, and the main phases were quartz, plagioclase, muscovite, and calcite. SS, CS, and FA had a high content of CaO (39.92%, 93.83%, 41.82%), while BFS had a high content of SiO<sub>2</sub> (39.83%). Additionally, SS contained 27.26% Fe<sub>2</sub>O<sub>3</sub>. The major components of DG were CaO (47.43%) and SO<sub>3</sub> (43.32%). As shown in Figure 1, the main phases of FA were quartz, mullite, CaO, and corundum. BFS is an amorphous phase structure. The dominant phases of SS were tetracalcium aluminoferrite C<sub>4</sub>AF (4CaO·Al<sub>2</sub>O<sub>3</sub>·Fe<sub>2</sub>O<sub>3</sub>), dicalcium silicate C<sub>2</sub>S (2CaO·SiO<sub>2</sub>), and tricalcium silicate C<sub>3</sub>S (3CaO·SiO<sub>2</sub>).

**Table 2.** Chemical composition of the test soil and the raw materials (wt. %).

|           | SiO <sub>2</sub> | Al <sub>2</sub> O <sub>3</sub> | CaO   | Fe <sub>2</sub> O <sub>3</sub> | MgO  | K <sub>2</sub> O | Na <sub>2</sub> O | Cl   | TiO <sub>2</sub> | SO <sub>3</sub> | LOI   |
|-----------|------------------|--------------------------------|-------|--------------------------------|------|------------------|-------------------|------|------------------|-----------------|-------|
| test soil | 52.93            | 18.55                          | 10.86 | 7.94                           | 3.45 | 3.66             | 0.88              | 0.08 | 0.94             | 0.1             | 1.21  |
| SS        | 15.04            | 2.36                           | 39.92 | 27.26                          | 7.84 | 0.03             | 0.44              | 0.23 | 0.82             | 0.23            | 2.92  |
| CS        | 2.46             | 1.71                           | 93.83 | 0.30                           | 0    | 0                | 0.53              | 0.67 | 0.05             | 0.36            | 26.84 |
| BFS       | 39.83            | 30.33                          | 14.52 | 7.92                           | 1.01 | 1.42             | 1.06              | 0    | 1.49             | 1.12            | 2.15  |
| DG        | 3.19             | 1.21                           | 47.43 | 1.19                           | 1.42 | 0.29             | 0.39              | 0.84 | 0.11             | 43.32           | 20.27 |
| FA        | 28.06            | 15.73                          | 41.82 | 1.60                           | 7.91 | 0.36             | 0.35              | 0.04 | 1.17             | 2.47            | 3.49  |

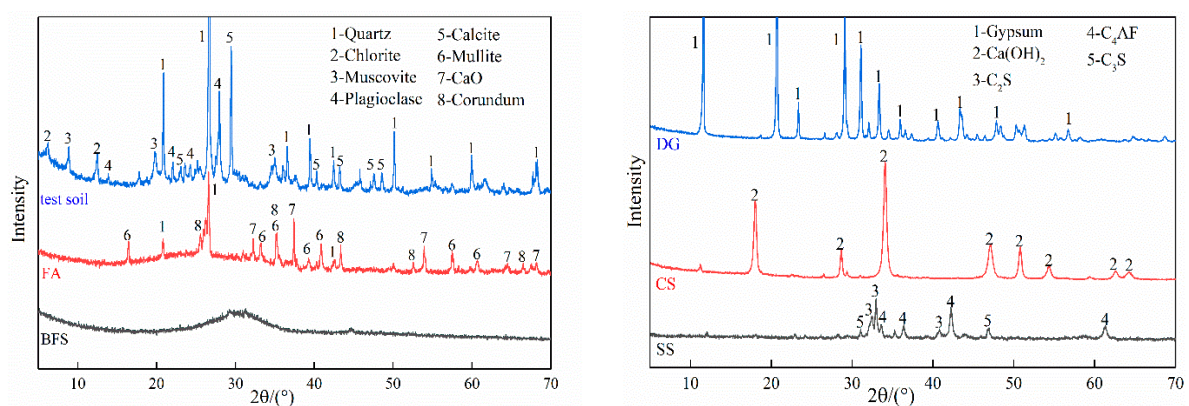


**Figure 1.** XRD patterns of the test soil and the raw materials.

## 2.2. Sample Preparation

The test soil was dried at a temperature of 55 °C and ground to a specific surface area reached 450–500 cm<sup>2</sup>/g. The MSWSS was produced by mixing CS, BFS, SS, FA, and DG in a certain proportion obtained using the D-optimal mixture design approach. The amount of the addition of MSWSS was fixed at 10% of the total mass of the test soil. Then, a certain amount of water was added, the MSWSS and test soil were mixed with the water, and the mixture

moisture content was 17.86%. Afterwards, the samples were prepared in accordance with the “Test Methods of Materials Stabilized with Inorganic Binders for Highway Engineering” (JTGE51-2009). The specimens were placed within a cylindrical mold with a diameter and height of 50mm and shaped by applying a stable pressure using a TYA-2000 digital display pressure testing machine at a loading rate of 1 mm/min for 2 min. Afterwards, the samples were weighed, enclosed within sealed bags, and moved to a standard environment with a relative humidity of over 95% and a temperature maintained at  $20 \pm 2$  °C for the specified curing time. After reaching the set time, the specimens were tested for compressive strength and microstructure characterization.

### 2.3. D-Optimal Mixture Design

The D-optimal mixture design is commonly used in experimental design to optimize multiple variables simultaneously. In this study, the optimal formulation of raw materials was determined using D-optimal design. The steel slag (SS), carbide slag (CS), blast furnace slag (BFS), desulfurized gypsum (DG), and fly ash (FA) were labelled as A, B, C, D, and E. The lower and upper limits of each component were proposed based on preliminary experiments: A (5–20 wt. %), B (20–50 wt. %), C (5–15 wt. %), D (5–20 wt. %), and E (10–25 wt. %). A 35-run D-optimal mixture design with multiple constraints on the component proportions was implemented by using Design-Expert software version 13.0 (Table 3). The combination of the components and the experimental results of 7d UCS are listed in Table 4.

**Table 3.** The variables and their constraints for D-optimal mixture design.

| Variables | Name                | Content/wt. % |      |
|-----------|---------------------|---------------|------|
|           |                     | Low           | High |
| A         | Steel slag          | 5             | 20   |
| B         | Carbide slag        | 20            | 50   |
| C         | Blast furnace slag  | 5             | 15   |
| D         | Desulfurized gypsum | 5             | 20   |
| E         | Fly ash             | 10            | 25   |

**Table 4.** Experimental design of the five components and the results for 7-day unconfined compressive strength (7d UCS).

| Number | The Ratio of Each Component/wt. % |      |      |      |      | 7d UCS/MPa |
|--------|-----------------------------------|------|------|------|------|------------|
|        | A                                 | B    | C    | D    | E    |            |
| 1      | 12.6                              | 50.0 | 10.3 | 9.2  | 17.9 | 1.28       |
| 2      | 13.0                              | 47.7 | 9.3  | 20.0 | 10.0 | 1.23       |
| 3      | 12.6                              | 50.0 | 10.3 | 9.2  | 17.9 | 1.23       |
| 4      | 20.0                              | 32.4 | 10.1 | 12.5 | 25.0 | 1.35       |
| 5      | 13.8                              | 31.4 | 15.0 | 18.3 | 21.5 | 1.15       |
| 6      | 20.0                              | 50.0 | 15.0 | 5.0  | 10.0 | 1.17       |
| 7      | 8.2                               | 37.7 | 11.6 | 17.5 | 25.0 | 1.28       |
| 8      | 8.2                               | 37.7 | 11.6 | 17.5 | 25.0 | 1.27       |
| 9      | 12.6                              | 50.0 | 10.3 | 9.2  | 17.9 | 1.26       |
| 10     | 13.8                              | 41.7 | 8.6  | 11.0 | 25.0 | 1.27       |
| 11     | 17.5                              | 41.5 | 15.0 | 5.0  | 21.0 | 1.22       |
| 12     | 5.0                               | 50.0 | 5.0  | 17.3 | 22.8 | 1.19       |
| 13     | 20.0                              | 32.8 | 11.6 | 20.0 | 15.6 | 1.10       |
| 14     | 5.0                               | 45.5 | 14.8 | 20.0 | 14.8 | 1.59       |
| 15     | 17.3                              | 23.0 | 15.0 | 19.7 | 25.0 | 1.01       |
| 16     | 15.3                              | 42.7 | 15.0 | 15.2 | 11.7 | 1.58       |
| 17     | 20.0                              | 41.0 | 10.5 | 11.4 | 17.1 | 1.15       |
| 18     | 20.0                              | 40.5 | 8.6  | 20.0 | 10.9 | 1.12       |
| 19     | 15.3                              | 42.7 | 15.0 | 15.2 | 11.7 | 1.53       |
| 20     | 20.0                              | 47.8 | 5.0  | 13.0 | 14.2 | 1.05       |

Table 4. Cont.

| Number | The Ratio of Each Component/wt. % |      |      |      |      | 7d UCS/MPa |
|--------|-----------------------------------|------|------|------|------|------------|
|        | A                                 | B    | C    | D    | E    |            |
| 21     | 15.6                              | 35.7 | 5.0  | 20.0 | 23.6 | 0.95       |
| 22     | 17.5                              | 41.5 | 15.0 | 5.0  | 21.0 | 1.21       |
| 23     | 5.0                               | 50.0 | 15.0 | 5.0  | 25.0 | 1.25       |
| 24     | 5.0                               | 44.4 | 15.0 | 12.9 | 22.7 | 1.63       |
| 25     | 20.0                              | 45.0 | 5.0  | 5.0  | 25.0 | 1.30       |
| 26     | 20.0                              | 25.0 | 10.0 | 20.0 | 25.0 | 1.06       |
| 27     | 12.8                              | 40.0 | 9.4  | 20.0 | 17.8 | 1.28       |
| 28     | 11.7                              | 50.0 | 5.0  | 8.3  | 25.0 | 1.03       |
| 29     | 10.0                              | 40.0 | 15.0 | 10.0 | 25.0 | 1.33       |
| 30     | 20.0                              | 50.0 | 8.3  | 5.0  | 16.7 | 1.12       |
| 31     | 12.8                              | 40.0 | 9.4  | 20.0 | 17.8 | 1.26       |
| 32     | 5.0                               | 50.0 | 15.0 | 15.0 | 15.0 | 1.64       |
| 33     | 18.3                              | 41.7 | 5.0  | 10.0 | 25.0 | 1.19       |
| 34     | 12.5                              | 50.0 | 15.0 | 12.5 | 10.0 | 1.54       |
| 35     | 13.2                              | 46.8 | 8.7  | 13.2 | 18.2 | 1.29       |

#### 2.4. Compressive Strength Test

The unconfined compressive strengths (UCS) were tested according to Chinese standard JTG E51-2009 [45] using an electro-hydraulic universal testing machine (CTS-E200) with a loading rate of 1mm/min. The measurements were performed on at least three representative samples to obtain an average value.

#### 2.5. X-ray Powder Diffraction (XRD)

The phase compositions of the samples were detected using the X-ray powder diffraction (XRD) method using a Bruker Advance D8 X-ray diffractometer with Cu K $\alpha$  radiation ( $\lambda = 0.1542$  nm) operating at 20 kV and 200 mA. The scanning angle ranged from 5° to 80°, with a scanning speed of 5°/min and a step size of 0.02°.

#### 2.6. Thermogravimetric Analysis (TGA)

Thermal analyses were performed on a thermogravimetric differential scanning calorimeter (TG-DSC, NETZSCH STA-409, Selb, Germany) with a nitrogen protective gas. A 30 mg sample was used for each measurement, with a heating rate of 10 °C/min in the temperature range of 25 to 1000 °C.

#### 2.7. Scanning Electron Microscopy (SEM)

Microstructural analysis of the specimens was performed using scanning electron microscopy (SEM) alongside an energy dispersive spectra (EDS) analyzer. EDS was utilized to determine the elemental composition of hydration products. SEM-EDS was conducted using a Zeiss SUPRA 55 field emission-scanning electron microscope (FE-SEM) outfitted with a LinkNA1000 energy spectrometer.

### 3. Results and Discussion

#### 3.1. Optimization of Mixture Composition for MSWSS

##### 3.1.1. Fitting Model and Response Surface Analysis

The interaction between the five components was mathematically modeled against the response to 7d UCS. A comparison and evaluation of different fitting models was performed using the Design-Expert 13 program. The assessment results of the accuracy of the four fitting models are shown in Table 5. The model selection criteria were a higher  $F$ -value, the adjusted and predicted  $R^2$  value, and a low  $p$ -value ( $<0.05$ ). According to the result, the special cubic model was selected. The  $p$ -value of the special cubic model was below 0.0001, suggesting that the model adequately describes the response. With a

coefficient of determination of  $R^2 = 0.9971$ , it can be inferred that the experimental data closely align with the predicted values, affirming the model’s high significance.

**Table 5.** Accuracy evaluation of different fitting models.

| Model         | Sequential <i>p</i> -Value | Lack of Fit <i>p</i> -Value | Adjusted R <sup>2</sup> | Predicted R <sup>2</sup> | Evaluate  |
|---------------|----------------------------|-----------------------------|-------------------------|--------------------------|-----------|
| Linear        | 0.0002                     | <0.0001                     | 0.4607                  | 0.2808                   |           |
| Quadratic     | 0.0002                     | 0.0008                      | 0.8162                  | 0.5376                   |           |
| Special Cubic | <0.0001                    | 0.8173                      | 0.9893                  | 0.8363                   | Suggested |
| Cubic         | 0.8173                     |                             | 0.9862                  |                          | Aliased   |

Analyses of variance (ANOVAs) were conducted on the response (7d UCS) using the Design-Expert software. The results of the ANOVAs for 7d UCS are shown in Table 6. The *p*-values and *F*-values represent the significance of variable factors. In general, smaller *p*-values (*p*-value > 0.05 insignificant, *p*-value < 0.05 significant, *p*-value < 0.01 extremely significant), along with larger *F*-values, denote the more significant impact of the variable factors on the response [46]. It can be seen from Table 6 that except for the interaction terms CD, CE, DE, ACD, and BCE, the *p*-values of other interaction terms were all < 0.01, which means that they had a notable influence on the 7d UCS. In contrast, interactive items CD, CE, DE, ACD, and BCE had no significant effects on 7d UCS because their *p*-values were greater than 0.05. Multiple quadratic regression equations were used to fit the functional relationship between the influencing variable factors and the responses. Equation (1) reflects the mathematical relations between 7d UCS and factors A, B, C, D, and E. The coefficients of the equation could be used to describe the effect of these variables on the response (7d UCS). A positive coefficient in the equation signifies a positive effect, while a negative coefficient indicates a negative effect. According to the results, the interactive terms AB, AD, AE, BC, BE, ABC, ABD, ABE, ADE, BCD, and BDE had an extremely significant effect (*p*-value < 0.01) on the 7d UCS.

$$\begin{aligned}
 Y_{7d\text{ UCS}} = & -16.15A + 2.32B - 4.69C + 2.33D - 6.08E + 38.77AB + 49.56AC + 33.14AD + 69.80AE + 20.40BC + \\
 & 8.38BD + 18.29BE - 4.67CD + 8.21CE + 8.67DE - 94.45ABC - 37.40ABD - 113.92ABE + 17.71ACD - \\
 & 44.35ACE - 90.85ADE + 38.52BCD - 4.88BCE + 21.40BDE + 3.81CDE
 \end{aligned}
 \tag{1}$$

**Table 6.** ANOVA table of experimental results.

| Source         | Sum of Squares | Free Degree | Mean Square | F-Value | <i>p</i> -Value |             |
|----------------|----------------|-------------|-------------|---------|-----------------|-------------|
| Model          | 1.07           | 24          | 0.0445      | 128.53  | <0.0001         | significant |
| Linear Mixture | 0.5633         | 4           | 0.1408      | 406.92  | <0.0001         |             |
| AB             | 0.0436         | 1           | 0.0436      | 125.97  | <0.0001         |             |
| AC             | 0.0083         | 1           | 0.0083      | 24.05   | 0.0008          |             |
| AD             | 0.0174         | 1           | 0.0174      | 50.15   | <0.0001         |             |
| AE             | 0.0543         | 1           | 0.0543      | 156.97  | <0.0001         |             |
| BC             | 0.0068         | 1           | 0.0068      | 19.72   | 0.0016          |             |
| BD             | 0.0028         | 1           | 0.0028      | 7.95    | 0.0200          |             |
| BE             | 0.0112         | 1           | 0.0112      | 32.42   | 0.0003          |             |
| CD             | 0.0001         | 1           | 0.0001      | 0.2386  | 0.6369          |             |
| CE             | 0.0002         | 1           | 0.0002      | 0.4495  | 0.5194          |             |
| DE             | 0.0012         | 1           | 0.0012      | 3.45    | 0.0960          |             |
| ABC            | 0.0171         | 1           | 0.0171      | 49.50   | <0.0001         |             |
| ABD            | 0.0099         | 1           | 0.0099      | 28.74   | 0.0005          |             |
| ABE            | 0.0658         | 1           | 0.0658      | 190.23  | <0.0001         |             |
| ACD            | 0.0004         | 1           | 0.0004      | 1.30    | 0.2841          |             |
| ACE            | 0.0014         | 1           | 0.0014      | 4.11    | 0.0733          |             |
| ADE            | 0.0284         | 1           | 0.0284      | 82.04   | <0.0001         |             |

Table 6. Cont.

| Source | Sum of Squares | Free Degree | Mean Square | F-Value | p-Value |
|--------|----------------|-------------|-------------|---------|---------|
| BCD    | 0.0038         | 1           | 0.0038      | 10.86   | 0.0093  |
| BCE    | 0.0000         | 1           | 0.0000      | 0.1022  | 0.7565  |
| BDE    | 0.0037         | 1           | 0.0037      | 10.83   | 0.0094  |

Table 7 presents the findings of the model reliability test analysis.  $R^2$  represents the correlation coefficient between the predicted and actual values. A higher  $R^2$  value indicates a stronger correlation. If the values of the adjusted  $R^2$  and predicted  $R^2$  are high and the difference between them is close (adjusted  $R^2$ -predicted  $R^2 < 0.2$ ), then the regression model can further prove this conclusion. As shown in Table 7, the values of  $R^2$ , adjusted  $R^2$ , predicted  $R^2$ , and adequate precision were 0.9971, 0.9893, 0.8363, and 43.2860, respectively. This indicated that the model equation can represent the relationship between the components and the 7d UCS well. The value of C.V. % was 1.48, indicating that the experiment shows high reliability and accuracy. The results showed that this model was able to predict the 7d UCS relatively accurately.

Table 7. Model reliability test analysis.

| Model               | Std. Dev. | Mean /MPa | C.V./% | $R^2$  | Adjusted $R^2$ | Predicted $R^2$ | Adequate Precision |
|---------------------|-----------|-----------|--------|--------|----------------|-----------------|--------------------|
| $Y_{7d\text{ UCS}}$ | 0.0186    | 1.26      | 1.48   | 0.9971 | 0.9893         | 0.8363          | 43.2860            |

The response surface interaction analysis was used to evaluate the effect of each raw material on the 7d UCS of the solidified soil. Figure 2 shows the 3D surface graphs and contour illustrating the impact of the independent variables on the 7d UCS. Generally, when the response surface shows a curved form, it indicates that there is a degree of interaction among the raw material components [46]. As seen in Figure 2, an increase in the dosage of desulfurized gypsum and blast furnace slag resulted in an increase in the 7d UCS, whereas an increase in the dosage of steel slag, carbide slag, and fly ash had the opposite effect.

### 3.1.2. Optimization of Mixture Composition

The maximum unconfined compressive strength value for 7 days (7d UCS) is used as the target optimization value. Based on regression model analysis combined with the 3D response surface plots and contour plots, the optimal ratio of the soil solidifier can be obtained. According to the predicted result, the optimal raw material proportion for preparing the MSWSS was: 5% steel slag, 50% carbide slag, 15% blast furnace slag, 15% desulfurized gypsum and 15% fly ash, respectively. The predicted value of the 7d UCS was 1.65 MPa. To confirm the precision of the predicted value, experiments on the compressive strength for 7 days were carried out. The outcome is displayed in Table 8. The experimental value closely aligned with the predicted value, which demonstrated the reliability of the model. The value of the absolute relative deviations was 1.81% (<5%), suggesting that the prediction model exhibits high accuracy.

Table 8. Comparison of the observed values and the predicted values after optimization.

| Proportion of Components/wt. % |    |    |    |    | 7d UCS/MPa      |                | Absolute Relative Deviations/% |
|--------------------------------|----|----|----|----|-----------------|----------------|--------------------------------|
| A                              | B  | C  | D  | E  | Predicted Value | Observed Value |                                |
| 5                              | 50 | 15 | 15 | 15 | 1.65            | 1.62           | 1.81                           |

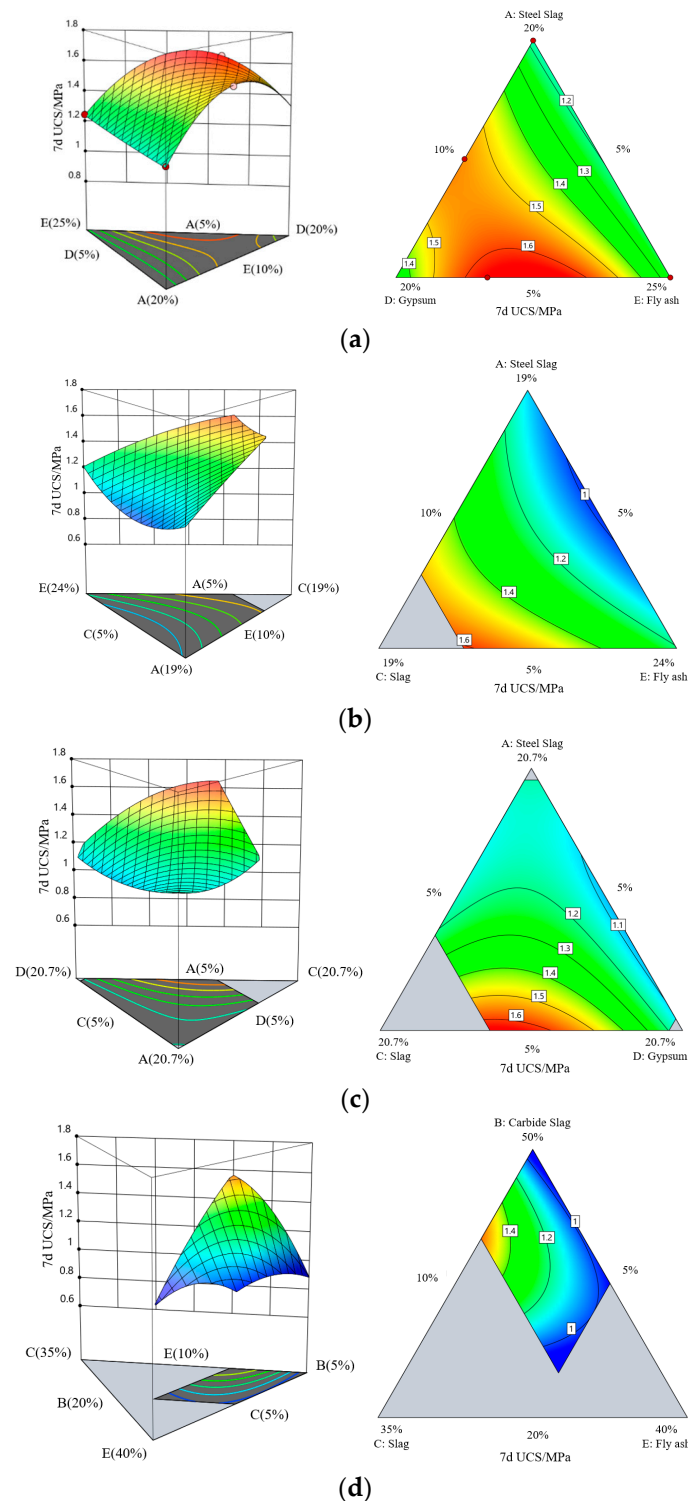


**Figure 2.** 3D surface graphs and contour plots for the effects of the independent variables on 7d UCS (A: Steel slag, B: Carbide slag, C: Blast furnace slag, D: Desulfurized gypsum, E: Fly ash): (a) the effect of A, D, E on 7d UCS; (b) the effect of A, C, E on 7d UCS; (c) the effect of A, C, D on 7d UCS; (d) the effect of B, C, E on 7d UCS.

### 3.2. Compressive Strength Test

MSWSS was prepared from multiple solid waste according to the optimal ratio obtained using the D-optimal mixture design method (SS:CS:BFS:DG:FA = 5:50:15:15:15). To compare the solidification effects of multiple solid waste-based stabilizer and ordinary

portland cement (OPC) on the test soil, the unconfined compressive strength (UCS) of these two stabilized soils was tested and analyzed. Standard specimens were prepared using the test soil plus 10% MSWSS, with a moisture content of 17.65%. In addition, 10% P.O32.5 OPC was used instead of MSWSS as a comparative experiment.

The unconfined compressive strength (UCS) of the stabilized soil at various curing ages is presented in Figure 3. The UCS of the stabilized soil showed a progressive increase with the curing time. The soil solidified using MSWSS has a UCS ranging from 0.35 MPa to 3.27 MPa. At the same time, soil solidified using OPC has a UCS ranging from 0.47 MPa to 2.89 MPa. The 7d UCS results of the MSWSS group and of the OPC group were 1.7 MPa and 1.25 MPa, respectively, which met the standard requirements of Chinese technical standards for the Technical Guidelines for Construction of Highway Roadbases. The 7d UCS of MSWSS-stabilized soil is 36% higher than that of the OPC group. It can be seen from Figure 3 that the UCS of OPC stabilized soil was higher than that of MSWSS-stabilized soil when the curing age is in the first 3 days. Afterwards, with the prolongation of curing time, the UCS of soil stabilized using MSWSS was significantly higher than that of the OPC group. After curing for 180 days, the compressive strength exhibited a notable increase to 3.27 MPa and 2.89 MPa, respectively.

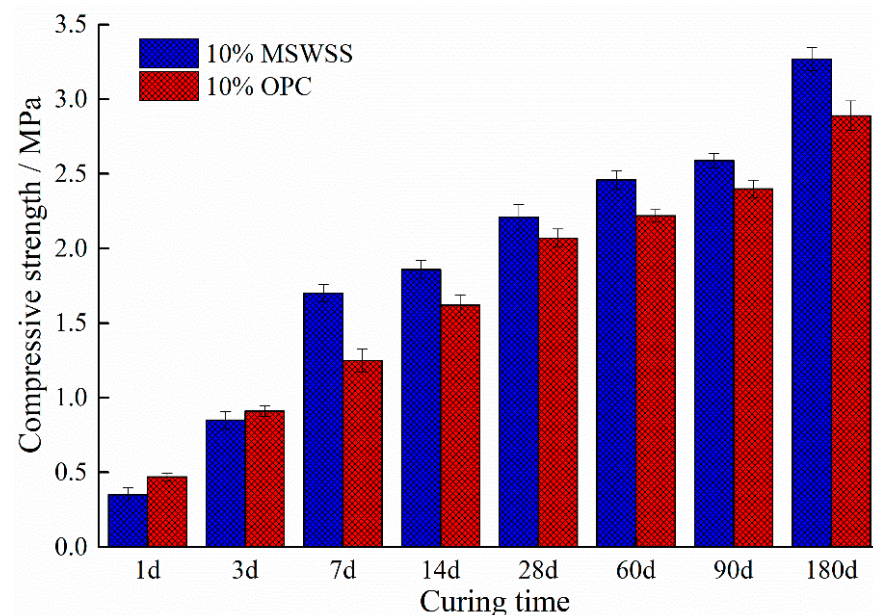


**Figure 3.** Compressive strength of stabilized soil at different curing times.

### 3.3. XRD Analysis

The XRD patterns of the solidified test soil at curing times of 7, 28, and 90 days are presented in Figure 4, and the primary phase compositions have been identified and labeled. Based on the results, the main phases were quartz, calcite, and plagioclase, and the primary hydration products were ettringite (AFt) and calcium silicate hydrate (C-S-H). This is consistent with the results of the SEM analysis (Figure 5). In addition, it also contained small amounts of chlorite and microcline. After curing for 7 days, ettringite and C-S-H can be observed from XRD pattern. As the curing time progressed, the intensity of AFt increased gradually, and the intensity of C-S-H also showed a weak increase, indicating that the hydration reaction was constantly developing. Meanwhile, a small amount of  $C_2S$  was detected, and the peak intensity decreased from 7 to 28 days of curing time, consistent with previous research [4,47]. Moreover, no distinct peaks of  $C_2S$  were observed after 90 days of curing. This showed that  $C_2S$  is involved in the hydration process. Generally, it was assumed that the hydration reaction of  $C_2S$  generated C-S-H.

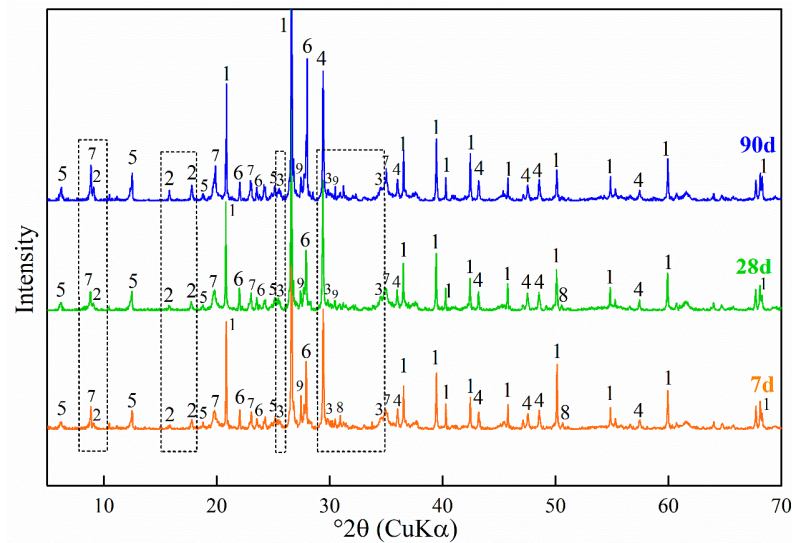


**Figure 4.** XRD patterns of stabilized soil with different curing times. 1-Quartz; 2-Ettringite (AFt); 3-C-S-H; 4-Calcite; 5-Chlorite; 6-Plagioclase; 7-MUCSovite; 8-C<sub>2</sub>S; 9-Microcline.

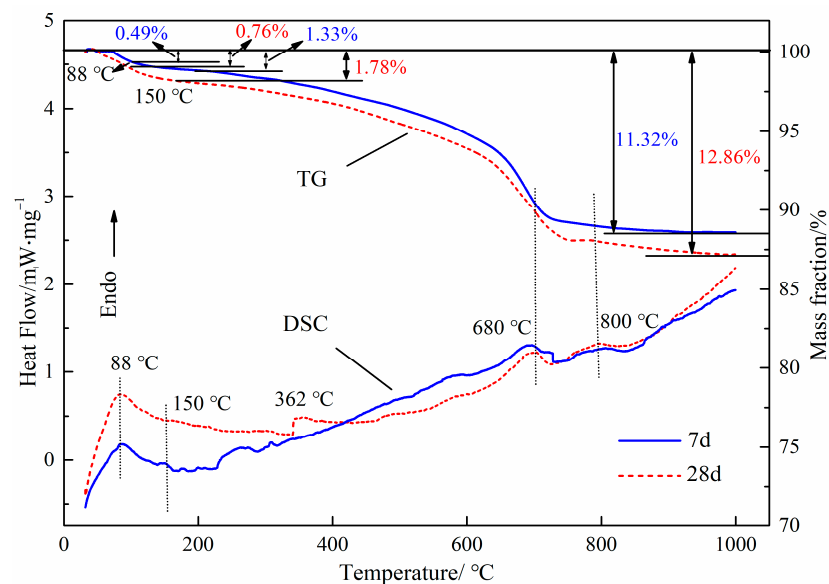


**Figure 5.** TG-DSC diagram of solidified soil at different curing times.

### 3.4. TG–DSC Analysis

The TG-DSC curves of the samples after curing for 7 and 28 days are displayed in Figure 5. The endothermic peaks at 50–400 °C could be primarily attributed to the thermal decomposition of C-S-H gel and AFt [24]. The endothermic peaks at 88 °C and 150 °C of the DSC curves were due to the release of free water [48]. The mass losses at 88 °C and 150 °C of the stabilized soil at 7 days and 28 days were 0.49% and 1.33%, and 0.76% and 1.78%, respectively. The endothermic peak at 362 °C of the DSC curves at a curing age of 28 days can be attributed to the dehydration of the crystal water of C-S-H and ettringite. The endothermic peaks at 680 °C and 800 °C were due to the decarburization and decomposition of calcite [25]. The results of the thermal analysis showed that the total mass loss of the samples after curing for 7 days and 28 days was 11.32% and 12.86%, respectively. This indicated that the hydration reaction continues as the curing age increases. The XRD analysis results also showed that the aggregate mass of the hydration products increases with the increase in curing time.

### 3.5. SEM-EDS Analysis

Figure 6 illustrates the microstructure of the solidified soils after 7 and 28 days of hydration. Figure 6a,b represent the samples at 7 curing days and 28 curing days. After curing for 7 days, the sample presented a loose arrangement and showed the typical needle-rod crystal structures of AFt (Figure 6a). Simultaneously, C-S-H gel was detected, which covered the needle-rod crystals of the AFt. The AFt crystals and C-S-H grew intertwined with each other, and this kind of structure could effectively improve the early compressive strength of the stabilized soil (Figure 3).

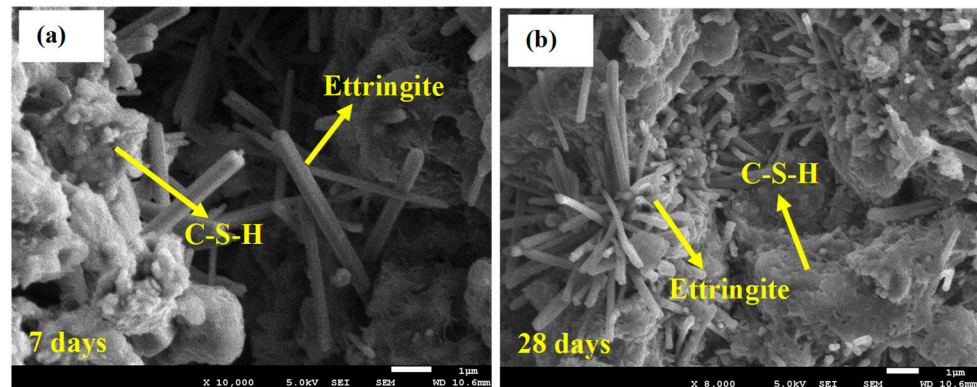
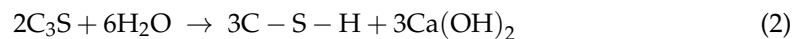


**Figure 6.** SEM morphology of the solidified soil for (a) 7 days and (b) 28 days curing times.

As the curing time progressed to 28 days (Figure 6b), the content of the needle-rod structures representing ettringite was increased, which corresponds with the findings of the XRD analysis. Meanwhile, the loosely structured solidified soil became denser, which might be attributed to the gradually increasing output of the C-S-H gel filling the pore space. At this stage, the AFt is surrounded by C-S-H gel, resulting in a significant enhancement in the compressive strength.

### 3.6. Discussion

According to characterization of the solidified soil, the primary hydration products were C-S-H gel ( $\text{Ca}_5\text{Si}_6\text{O}_{16}(\text{OH})\cdot 4\text{H}_2\text{O}$ ) and AFt ( $3\text{CaO}\cdot\text{Al}_2\text{O}_3\cdot 3\text{CaSO}_4\cdot 32\text{H}_2\text{O}$ ). Carbide slag (CS) plays a crucial role in the hydration process because it provides  $\text{Ca}^{2+}$  ions and an alkaline environment. At the initial phase of hydration, the  $\text{C}_2\text{S}$  ( $2\text{CaO}\cdot\text{SiO}_2$ ) and  $\text{C}_3\text{S}$  ( $3\text{CaO}\cdot\text{SiO}_2$ ) in SS were hydrolyzed to form C-S-H gel and calcium hydroxide ( $\text{Ca}(\text{OH})_2$ ) (Equations (2) and (3)), which improved the early compressive strength (Figure 3). Meanwhile, a notable quantity of  $\text{Ca}(\text{OH})_2$  was produced, raising the alkalinity of the binder.



In alkaline environments,  $\text{OH}^-$  reacts with the amphoteric oxide  $\text{Al}_2\text{O}_3$  and acidic oxide  $\text{SiO}_2$  which can accelerate the hydrolysis of the glass phase, destroying the Ca-O, Si-O, and Al-O bonds and form  $[\text{Al}(\text{OH})_6]^{3-}$  and  $[\text{Si}(\text{OH})_3]^-$  [49]. Subsequently, with the participation of the  $\text{Ca}^{2+}$  and  $\text{SO}_4^{2-}$  produced by the hydrolysis of DG, it reacts with  $[\text{Al}(\text{OH})_6]^{3-}$  and  $[\text{Si}(\text{OH})_3]^-$  to generate AFt. At the same time,  $[\text{Si}(\text{OH})_3]^-$  could react with  $\text{Ca}^{2+}$  to generate C-S-H gel. With the progression of the hydration reaction, the content of C-S-H and AFt increased significantly (Figure 4). The chemical reaction can be expressed in Equations (4)–(7). Consequently, large amounts of C-S-H and AFt grew interlacedly, filling the gaps between soil particles and improving the compactness and strength of the solidified soil. The hydration mechanism of the MSWSS is shown in Figure 7.



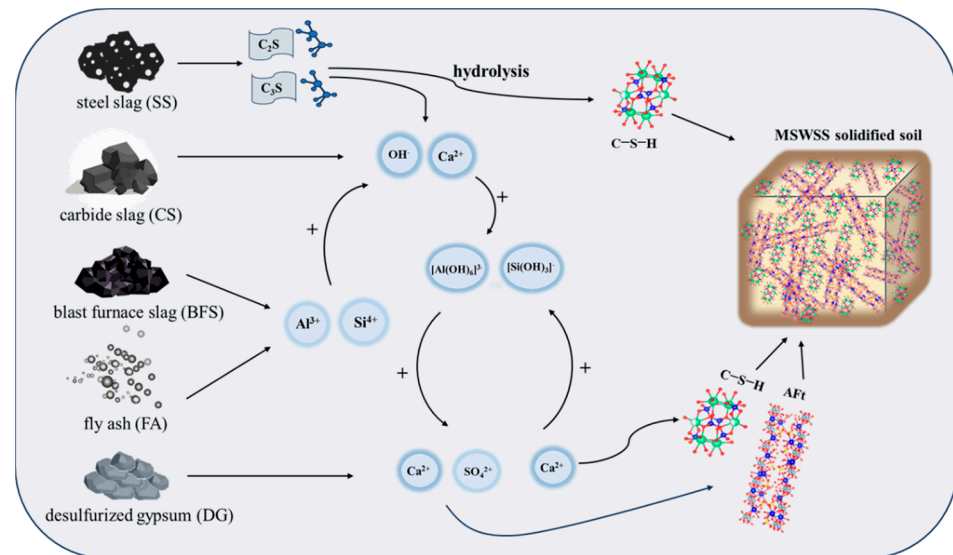
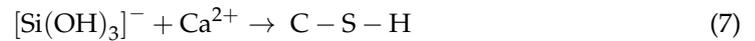
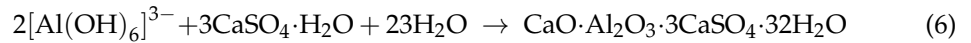
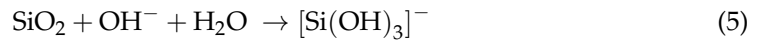


**Figure 7.** Hydration mechanism of the multiple industrial solid waste-based soil stabilizer (MSWSS).

#### 4. Conclusions

This study proposed the preparation of a multiple industrial solid waste-based soil stabilizer (MSWSS) using steel slag (SS), carbide slag (CS), blast furnace slag (BFS), fly ash (FA), and desulfurized gypsum (DG). The D-optimal mixture approach was utilized in the experimental design to obtain the optimal formulation of raw materials. The unconfined compressive strength (UCS) of the solidified test soil was evaluated, and the hydration mechanism was analyzed using the XRD, TG-DSC, and SEM methods. In summary, the following conclusions can be drawn:

- (1) Interaction between the five components was modeled mathematically against the responses of 7d UCS. According to the result of the ANOVA and the model reliability analysis, the prediction model showed a lower  $p$ -value ( $<0.0001$ ) and lower absolute relative deviations (1.81%), and a higher F-value (406.92), R2 value (0.9971), and adjusted R2 value (0.9893). This indicated that the model had high reliability and was able to predict 7d UCS relatively accurately.
- (2) The D-optimal mixture approach indicated that the optimal ratio of MSWSS should be 5% steel slag (SS), 50% carbide slag (CS), 15% blast furnace slag (BFS), 15% desulfurized gypsum (DG), and 15% fly ash (FA). The UCS of the stabilized soil increased with the curing time. The 7d UCS of soil stabilized using the multiple industrial solid waste-based soil stabilizer was 1.7 MPa and the 180d UCS increased to 3.27 MPa, which all met the requirements for the “Technical Guidelines for Construction of Highway Roadbases”. The UCS of the MSWSS stabilized test soil group was significantly higher than that of the OPC group.
- (3) XRD, TG-DSC, and SEM results revealed that the primary hydration products were Aft and C-S-H gel. As the curing progressed, the content of the Aft and C-S-H increased and the microstructure of stabilized soil exhibited a denser structure, leading to better mechanical strength.

The research proposed a novel low-carbon and environmentally friendly soil stabilizer, MSWSS, based on multiple industrial solid waste products, which could achieve better mechanical properties than traditional OPC stabilizers and meet the requirements of highway

construction. This technology has the potential to enhance the comprehensive utilization of industrial solid waste and contribute to environmental protection.

**Author Contributions:** Conceptualization, X.W. (Xiaoli Wang), X.W. (Xiancong Wang), and P.F.; methodology, investigation, data curation, X.W. (Xiaoli Wang), X.W. (Xiancong Wang), B.L., J.S. and M.X.; writing—original draft preparation, X.W. (Xiaoli Wang) and X.W. (Xiancong Wang); writing—review and editing, X.W. (Xiaoli Wang) and P.F.; supervision, project administration, P.F.; funding acquisition, X.W. (Xiaoli Wang) and P.F. All authors have read and agreed to the published version of the manuscript.

**Funding:** This research was funded by Key Research and Development Program of Hebei Province (grant numbers 22373809D), National Key Research and Development Program of China (grant numbers 2018YFC1900604), and Open Foundation of State Key Laboratory of Mineral Processing (grant numbers BGRIMM-KJSKL-2022-22).

**Data Availability Statement:** The data presented in this study are available on request from the corresponding author.

**Conflicts of Interest:** Authors Jinjin Shi and Miao Xu were employed by the Cangzhou Municipal Engineering Company Limited. The remaining authors declare that the research was conducted in the absence of any commercial or financial relationships that could be construed as a potential conflict of interest.

## References

- World Bank Group. *Trends in Solid Waste Management*; The World Bank: Bretton Woods, NH, USA, 2020; Available online: [https://datatopics.worldbank.org/what-a-waste/trends\\_in\\_solid\\_waste\\_management.html](https://datatopics.worldbank.org/what-a-waste/trends_in_solid_waste_management.html) (accessed on 9 February 2024).
- Guo, Y.; Glad, T.; Zhong, Z.Z.; He, R.N.; Tian, J.P.; Chen, L.J. Environmental life-cycle assessment of municipal solid waste incineration stocks in Chinese industrial parks. *Resour. Conserv. Recycl.* **2018**, *139*, 387–395. [[CrossRef](#)]
- Liu, A.; Ren, F.; Lin, W.L.Y.; Wang, J.Y. A review of municipal solid waste environmental standards with a focus on incinerator residues. *Int. J. Sustain. Built Environ.* **2015**, *4*, 165–188. [[CrossRef](#)]
- Wang, X.; Fu, P.; Deng, W.; Shi, J.; Xu, M. Study on Mechanism of MSWI Fly Ash Solidified by Multiple Solid Waste-Based Cementitious Material Using the Rietveld Method. *Processes* **2023**, *11*, 2311. [[CrossRef](#)]
- Kumar, R.A.; Singh, G.; Kumar, T.A. Comparative study of soil stabilization with glass powder, plastic and e-waste: A review. *Mater. Today Proc.* **2020**, *32*, 771–776. [[CrossRef](#)]
- Lu, J.Z.; Jiang, S.; Chen, J.J.; Lee, C.H.; Cai, Z.W.; Ruan, H.D. Fabrication of superhydrophobic soil stabilizers derived from solid wastes applied for road construction: A review. *Transp. Geotech.* **2023**, *40*, 100974. [[CrossRef](#)]
- Soltani-Jigheh, H.; Tahaei, Y.S.N. Effect of liquid polymer on properties of fine-grained soils. *Geotech. Eng.* **2019**, *50*, 9–21.
- Hassan, N.; Hassan, W.H.W.; Rashid, A.S.A.; Latifi, N.; Yunus, N.Z.M.; Horpibulsuk, S.; Moayed, H. Microstructural characteristics of organic soils treated with biomass silica stabilizer. *Environ. Earth Sci.* **2019**, *78*, 367. [[CrossRef](#)]
- Zhang, M.; Guo, H.; El-Korchi, T.; Zhang, G.; Tao, M. Experimental feasibility study of geopolymer as the next-generation soil stabilizer. *Constr. Build. Mater.* **2013**, *47*, 1468–1478. [[CrossRef](#)]
- Latifi, N.; Vahedifard, F.; Ghazanfari, E.; Rashid, A.S.A. Sustainable Usage of Calcium Carbide Residue for Stabilization of Clays. *J. Mater. Civ. Eng.* **2018**, *30*, 2313. [[CrossRef](#)]
- Latifi, N.; Vahedifard, F.; Siddiqua, S.; Horpibulsuk, S. Solidification–Stabilization of Heavy Metal–Contaminated Clays Using Gypsum: Multiscale Assessment. *Int. J. Géoméch.* **2018**, *18*, 1283. [[CrossRef](#)]
- Kavak, A.; Akyarlı, A. A field application for lime stabilization. *Environ. Geol.* **2007**, *15*, 987–997. [[CrossRef](#)]
- Ninov, J.; Donchev, I. Lime stabilization of clay from the ‘Mirkovo’ deposit. *J. Therm. Anal. Calorim.* **2008**, *19*, 487–490. [[CrossRef](#)]
- Tayeh, B.A.; Hasaniyah, M.W.; Zeyad, A.M.; Awad, M.M.; Alaskar, A.; Mohamed, A.M.; Alyousef, R. Durability and mechanical properties of seashell partially-replaced cement. *J. Build. Eng.* **2020**, *31*, 101328. [[CrossRef](#)]
- Marvila, M.T.; Alexandre, J.; Azevedo, A.R.G.; Zanelato, E.B.; Xavier, G.C.; Monteiro, S.N. Study on the replacement of the hydrated lime by kaolinitic clay in mortars. *Adv. Appl. Ceram.* **2019**, *118*, 373–380. [[CrossRef](#)]
- Latifi, N.; Vahedifard, F.; Ghazanfari, E.; Horpibulsuk, S.; Marto, A.; Williams, J. Sustainable Improvement of Clays Using Low-Carbon Nontraditional Additive. *Int. J. Géoméch.* **2018**, *18*, 1086. [[CrossRef](#)]
- Wang, L.; Chen, S.S.; Tsang, D.C.W.; Poon, C.; Shih, K. Recycling contaminated wood into eco-friendly particleboard using green cement and carbon dioxide curing. *J. Clean. Prod.* **2016**, *137*, 861–870. [[CrossRef](#)]
- Gu, J.; Liu, X.; Zhang, Z. Road base materials prepared by multi-industrial solid wastes in China: A review. *Constr. Build. Mater.* **2023**, *373*, 130860. [[CrossRef](#)]
- Rafiean, A.H.; Kani, E.N.; Haddad, A. Mechanical and Durability Properties of Poorly Graded Sandy Soil Stabilized with Activated Slag. *J. Mater. Civ. Eng.* **2020**, *32*, 2990.

20. Ghaffar, H.; Al-Kheetan, M.; Ewens, P.; Wang, T.; Zhuang, J. Investigation of the interfacial bonding between flax/wool twine and various cementitious matrices in mortar composites. *Constr. Build. Mater.* **2020**, *239*, 117833. [[CrossRef](#)]
21. Thirumalai, R.; Babu, S.S.; Naveennayak, V.; Nirmal, R.; Lokesh, G. A Review on Stabilization of Expansive Soil Using Industrial Solid Wastes. *Engineering* **2017**, *9*, 1008–1017. [[CrossRef](#)]
22. Zhang, J.; Li, S.; Li, Z. Investigation the synergistic effects in quaternary binder containing red mud, blast furnace slag, steel slag and flue gas desulfurization gypsum based on artificial neural networks. *J. Clean. Prod.* **2020**, *273*, 122972. [[CrossRef](#)]
23. Traven, K.; Češnovar, M.; Ducman, V. Particle size manipulation as an influential parameter in the development of mechanical properties in electric arc furnace slag-based AAM. *Ceram. Int.* **2019**, *45*, 22632–22641. [[CrossRef](#)]
24. Li, W.; Yi, Y. Use of carbide slag from acetylene industry for activation of ground granulated blast-furnace slag. *Constr. Build. Mater.* **2020**, *238*, 117713. [[CrossRef](#)]
25. Gao, D.; Zhang, Z.; Meng, Y.; Tang, J.; Yang, L. Effect of Flue Gas Desulfurization Gypsum on the Properties of Calcium Sulfoaluminate Cement Blended with Ground Granulated Blast Furnace Slag. *Materials* **2021**, *14*, 382. [[CrossRef](#)] [[PubMed](#)]
26. Wang, J.; Fu, H.; Yan, X.; Wang, L.; Wang, P. Research status of comprehensive utilization of steel slag. *China Nonferr. Metall.* **2021**, *50*, 77–82.
27. Wang, S.J.; Bu, H.T.; Chen, H.J.; Hu, T.; Chen, W.Z.; Wu, J.H.; Hu, H.J.; Lin, M.Z.; Li, Y.T.; Jiang, G.B. Floatable magnetic aerogel based on alkaline residue used for the convenient removal of heavy metals from wastewater. *Chem. Eng. J.* **2020**, *399*, 125760. [[CrossRef](#)]
28. Nan, J.K.; Chen, X.M.; Wang, X.Y.; Lashari, M.S.; Wang, Y.M.; Guo, Z.C.; Du, Z.J. Effects of applying flue gas desulfurization gypsum and humic acid on soil physicochemical properties and rapeseed yield of a saline-sodic cropland in the eastern coastal area of China. *J. Soils Sediments* **2016**, *16*, 38–50. [[CrossRef](#)]
29. Wang, X.; Kim, S.; Wu, Y.; Liu, Y.; Liu, T.; Wang, Y. Study on the optimization and performance of GFC soil stabilizer based on response surface methodology in soft soil stabilization. *Soils Found.* **2023**, *63*, 101278. [[CrossRef](#)]
30. Amran, M.; Debbarma, S.; Ozbakkaloglu, T. Fly ash-based eco-friendly geopolymer concrete: A critical review of the long-term durability properties. *Constr. Build. Mater.* **2021**, *270*, 121857. [[CrossRef](#)]
31. Makarichi, L.; Jutidamrongphan, W.; Techato, K.A. The evolution of waste-to-energy incineration: A review. *Renew. Sustain. Energy Rev.* **2018**, *91*, 812–821. [[CrossRef](#)]
32. Mao, Y.; Wu, H.; Wang, W.; Jia, M.; Che, X. Pretreatment of municipal solid waste incineration fly ash and preparation of solid waste source sulphoaluminate cementitious material. *J. Hazard. Mater.* **2020**, *385*, 121580. [[CrossRef](#)]
33. Chen, R.; Zhang, R.; Han, H. Climate neutral in agricultural production system: A regional case from China. *Environ. Sci. Pollut. Res.* **2021**, *28*, 33682–33697. [[CrossRef](#)]
34. Marieta, C.; Guerrero, A.; Leon, I. Municipal solid waste incineration fly ash to produce eco-friendly binders for sustainable building construction. *Waste Manag.* **2021**, *120*, 114–124. [[CrossRef](#)]
35. Wang, N.N.; Sun, X.Y.; Zhao, Q.; Yang, Y.; Wang, P. Leachability and adverse effects of coal fly ash: A review. *J. Hazard. Mater.* **2020**, *396*, 122725. [[CrossRef](#)]
36. Ren, C.; Wang, W.; Li, G. Preparation of high-performance cementitious materials from industrial solid waste. *Constr. Build. Mater.* **2017**, *152*, 39–47. [[CrossRef](#)]
37. Yang, J.; Zeng, J.; He, X.; Zhang, Y.; Su, Y.; Tan, H. Sustainable clinker-free solid waste binder produced from wet-ground granulated blast-furnace slag, phosphogypsum and carbide slag. *Constr. Build. Mater.* **2022**, *330*, 127218. [[CrossRef](#)]
38. Kampala, A.; Horpibulsuk, S. Engineering Properties of Silty Clay Stabilized with Calcium Carbide Residue. *J. Mater. Civ. Eng.* **2013**, *25*, 632–644. [[CrossRef](#)]
39. Yi, Y.; Gu, L.; Liu, S.; Puppala, A.J. Carbide slag-activated ground granulated blastfurnace slag for soft clay stabilization. *Can. Geotech. J.* **2015**, *52*, 656–663. [[CrossRef](#)]
40. He, J.; Shi, X.K.; Li, Z.X.; Zhang, L.; Feng, X.Y.; Zhou, L.R. Strength properties of dredged soil at high water content treated with soda residue, carbide slag, and ground granulated blast furnace slag. *Constr. Build. Mater.* **2020**, *242*, 118126. [[CrossRef](#)]
41. Ren, P.; Ling, T.C. Roles of chlorine and sulphate in MSWIFA in GGBFS binder: Hydration, mechanical properties and stabilization considerations. *Environ. Pollut.* **2021**, *284*, 117175. [[CrossRef](#)]
42. Wen, N.; Zhao, Y.; Yu, Z.; Liu, M. A sludge and modified rice husk ash-based geopolymer: Synthesis and characterization analysis. *J. Clean. Prod.* **2019**, *226*, 805–814. [[CrossRef](#)]
43. Phummiphan, I.; Horpibulsuk, S.; Phoongernkham, T.; Arulrajah, A.; Shen, S.L. Marginal Lateritic Soil Stabilized with Calcium Carbide Residue and Fly Ash Geopolymers as a Sustainable Pavement Base Material. *J. Mater. Civ. Eng.* **2017**, *29*, 1708. [[CrossRef](#)]
44. Venkatesan, M.; Zaib, Q.; Shah, I.H.; Park, H.S. Optimum utilization of waste foundry sand and fly ash for geopolymer concrete synthesis using D-optimal mixture design of experiments. *Resour. Conserv. Recycl.* **2019**, *148*, 114–123. [[CrossRef](#)]
45. Lei, B.; Fu, P.; Wang, X.; Ni, W.; Zhang, S.; Wang, X.; Shi, J.; Xu, M. The Hydration Mechanisms of Co-Stabilization Saline Soils by Using Multiple Solid Wastes. *Processes* **2023**, *11*, 2679. [[CrossRef](#)]
46. Asadzadeh, S.; Khoshbayan, S. Multi-objective optimization of influential factors on production process of foamed concrete using Box-Behnken approach. *Constr. Build. Mater.* **2018**, *170*, 101–110. [[CrossRef](#)]
47. Xu, C.; Ni, W.; Li, K.; Zhang, S.; Xu, D. Activation mechanisms of three types of industrial by-product gypsums on steel slag-granulated blast furnace slag-based binders. *Constr. Build. Mater.* **2021**, *288*, 123111. [[CrossRef](#)]

- 
48. Durdziński, P.T. *Hydration of Multi-Component Cements Containing Cement Clinker, Slag, Calcareous Fly Ash and Limestone*; EPFL: Lausanne, Switzerland, 2016; p. 189.
  49. Zhang, N.; Li, H.; Liu, X. Hydration mechanism and leaching behavior of bauxitecalcination-method red mud-coal gangue based cementitious materials. *J. Hazard. Mater.* **2016**, *314*, 172–180. [[CrossRef](#)]

**Disclaimer/Publisher’s Note:** The statements, opinions and data contained in all publications are solely those of the individual author(s) and contributor(s) and not of MDPI and/or the editor(s). MDPI and/or the editor(s) disclaim responsibility for any injury to people or property resulting from any ideas, methods, instructions or products referred to in the content.